Morphology and texture of particles along the Spirit rover traverse from sol 450 to sol 745

R. A. Yingst,[1] L. Crumpler,[2] W. H. Farrand,[3] R. Li,[4] N. A. Cabrol,[5,6] and L. D. Neakrase[7]

Received 29 April 2008; revised 16 September 2008; accepted 9 October 2008; published 20 December 2008.

[1] We quantified and classified the shape, roundness, size, and texture of 935 loose surface particles along the Spirit rover traverse from sols 450–745 to assess origin, transport, and other alteration mechanisms that altered particles during and after formation. Variation in particle morphologic parameters along traverse is consistent with crossing mapped geologic unit boundaries. Texture is divided into four types: vesicular, smooth and flat-faceted, rough and flat-faceted, and very rough. Sphericity and roundness are intermediate and low, respectively, comparable to particles moved by high-energy transport or to crushed particles. This indicates intermittent, high-energy emplacement or modification of a single lithology, rather than systematic, continuous low-energy abrasion or wear over time. Comparison with particle morphology at other Mars landing sites is consistent with the hypothesis that no secondary systematic transport or wide-scale chemical alteration was active at a significant enough level to alter macromorphology. In particular, particle morphology at the Mars Pathfinder site shows stronger evidence of abrasion than along the Spirit traverse, suggesting Mars Pathfinder particles have undergone abrasion processes that particles in this study area have not. Additionally, morphology indices have correlation coefficients near zero, indicating that a fluvial transport mechanism is likely not responsible for morphology. Morphology and texture are instead related to origin and composition rather than subsequent modification. Morphology and texture support a volcanic origin, possibly without modification, but most likely altered primarily by ballistic impact, implying that the Spirit landing site and traverse may be utilized in the future as a standard site for characterization of impact-derived morphology.

Citation: Yingst, R. A., L. Crumpler, W. H. Farrand, R. Li, N. A. Cabrol, and L. D. Neakrase (2008), Morphology and texture of particles along the Spirit rover traverse from sol 450 to sol 745, *J. Geophys. Res.*, *113*, E12S41, doi:10.1029/2008JE003179.

1. Introduction

[2] A primary science objective of the Mars Exploration Rover (MER) mission is to determine the geologic context of the consolidated materials that lie along each rover's path [*Crisp et al.*, 2003]. The Spirit rover instrument payload has revealed a landscape awash in surface particles characterized by diverse sizes, morphologies and textures [*Squyres et al.*, 2004; *Crumpler et al.*, 2005a; *Arvidson et al.*, 2006; *Cabrol et al.*, 2006; *Golombek et al.*, 2006]. (In the following sections, the term particle refers to rock fragments in the pebble to cobble size range [*Wentworth*, 1922] and the term "macromorphology" refers to a particle's characteristics at the multimillimeter scale.) Determining the origin and history of these loose particles requires relating their physical characteristics to likely scenarios of emplacement and subsequent wear.

[3] The macromorphologic characteristics of loose surface particles provide a record of their original lithology and the sorting and abrasive processes that altered them [*Wadell*, 1932, 1933; *Krumbein and Sloss*, 1963; *Pettijohn*, 1975]. On Earth, morphological characteristics such as shape, texture, fabric and roundness are commonly used to help determine important aspects of a particle's origin and abrasion history (transport, deposition and wear), even in locations where the source outcrop is not immediately obvious [e.g., *Dobkins and Folk*, 1970]. Because they can be assessed qualitatively and quantitatively to a high degree of accuracy [*Krumbein*, 1941a, 1941b; *Pettijohn*, 1975], morphologic characteristics have the potential to give meaning to physical characteristics where certain other factors are known. For example, the distance traveled by a particle from its source may be determined from morphology if the source and transport mechanism are well modeled [*Boulton*, 1978; *Howard*, 1992]. In terrestrial settings where

[1]Department of Natural and Applied Sciences, University of Wisconsin-Green Bay, Green Bay, Wisconsin, USA.
[2]New Mexico Museum of Natural History and Science, Albuquerque, New Mexico, USA.
[3]Space Science Institute, Boulder, Colorado, USA.
[4]Department of Civil Engineering, Ohio State University, Columbus, Ohio, USA.
[5]Space Science Division, NASA Ames Research Center, Moffett Field, California, USA.
[6]SETI Carl Sagan Center, Mountain View, California, USA.
[7]School of Earth and Space Exploration, Arizona State University, Tempe, Arizona, USA.

0148-0227/08/2008JE003179

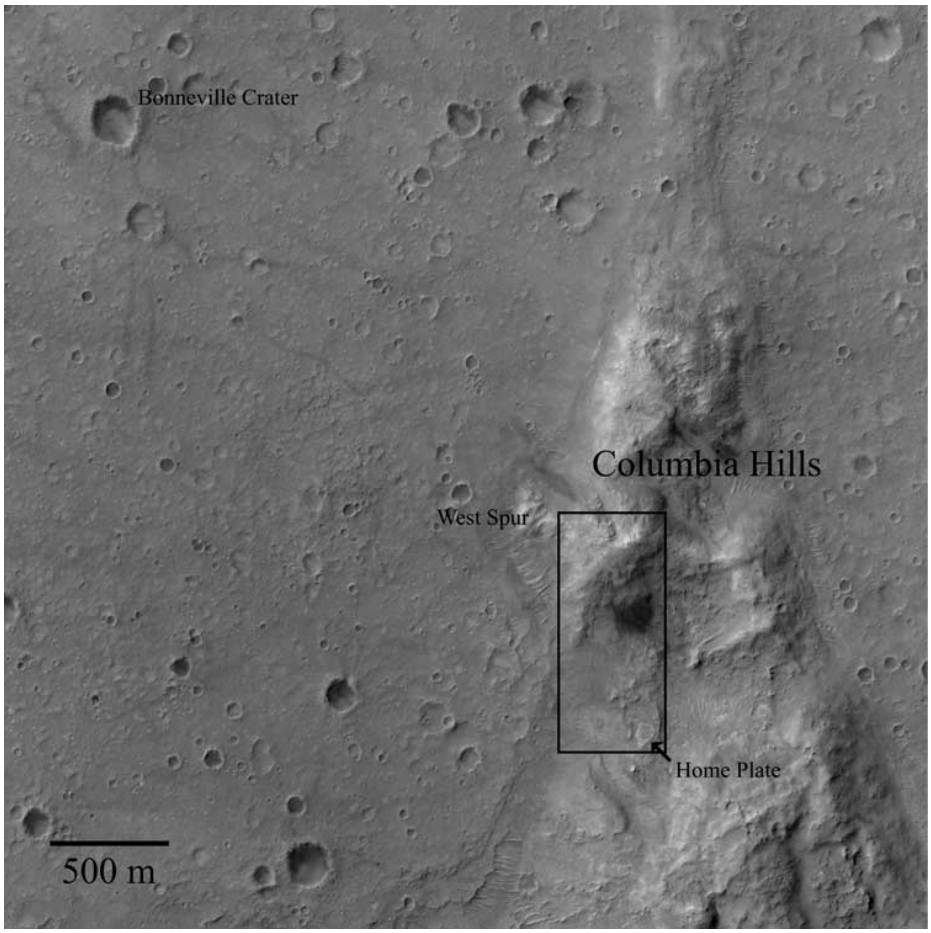

Figure 1. Mars Reconnaissance Orbiter/High Resolution Imaging Science Experiment (HiRISE) image PSP_001513_1655 of the Spirit traverse area, with major landmarks noted. North is up in this image; boxed area is the traverse region, shown in Figure 2.

the source is known but numerous wear mechanisms are active, the shape and roundness of worn particles may be reliably predicted from standard populations, so that particles of uncertain history may be classified [*Dobkins and Folk*, 1970]. Morphological characteristics also yield a metric for classifying particle populations, an especially important element in environments for which source outcrops cannot be characterized in detail.

[4] Earlier Mars missions returned images of sufficient quality to provide particle data in two dimensions, enough to characterize morphology in a static location and make first-order conclusions regarding particle lithology and mechanisms involved in their transport [*Garvin et al.*, 1981; *Basilevsky et al.*, 1999a, 1999b; *Yingst et al.*, 2007]. The MER mission represents the first opportunity for systematic characterization and analysis of a statistically significant number of particles on Mars as they occur along a substantial length of the surface, enabling the mapping of changes in morphology and texture with lateral distance. Any detected changes in particle characteristics along traverse would indicate possible changes in point of origin, primary transport process or subsequent in situ breakdown processes [e.g., *Cabrol et al.*, 2006, 2008; *Grant et al.*, 2006a]. On Earth transport distance and other particle information are often based on what is known of the primary environment or process involved in creating or transporting the particle. In Gusev Crater, we work backward, using particle characteristics to yield clues to their origin, emplacement and wear. Here, we report on an analysis of quantitative morphologic characteristics of surface particles (also termed float) in Gusev Crater imaged along the traverse of the Spirit rover from sols 450 to 745. From this analysis we suggest an origin, nature and geologic history for these particles, and their variance by location.

2. Geologic Setting

[5] Spirit landed in Gusev crater, a 160-km diameter, early to middle Noachian-aged crater situated 300 km south of the Apollinaris Patera volcanic shield [*Cabrol et al.*, 1996, 1998a, 1998b; *Kuzmin et al.*, 2000] (Figure 1). The crater floor is dominated by plains deposits originally interpreted to be sediments laid down from two sources during prolonged fluviolacustrine activity [*Cabrol et al.*, 1996, 1998a, 1998b; *Kuzmin et al.*, 2000; *Cabrol et al.*, 2003]. The first source consists of small valley networks along the eastern and southern crater rim; these deposited aqueous sediment through the late Noachian. The second,

larger source is Ma'adim Vallis, an 800-km long early Hesperian channel that drained through the highlands and breached the crater's south rim, generating fluviolacustrine deposits during discontinuous activity throughout the Hesperian. The presence of a viscous, laminar flow feature running from the Ma'adim Vallis breach nearly 150 km across the crater floor [*Rice et al.*, 2003] strongly suggests a fluvial origin for at least some of the materials on the Gusev floor.

[6] However, data from the Athena science package have revealed that the Spirit landing site in Gusev Crater is dominated by basalt flows modified by small impact craters [*Golombek et al.*, 2006]. Materials from the surface down to at least 1–2 m on the basalt flows [*Crumpler et al.*, 2005b], and possibly down to ~10 m depth in the hills, are interpreted to be impact-generated regolith [*Grant et al.*, 2004; *Squyres et al.*, 2004; *Arvidson et al.*, 2006; *Golombek et al.*, 2006]. Low-relief rocky plains dominate the landscape, punctuated by shallow soil-filled circular hollows with rocky rims (common around the Bonneville region), interpreted to be eroded impact structures [*Golombek et al.*, 2006; *Grant et al.*, 2006a]. The site is also peppered with smaller craters 0.4–400 m in diameter. Eolian activity is characterized by organized, preferentially oriented soil bed forms, ripples, wind abrasion features on rocks and outcrops, and perched and buried rocks [*Greeley et al.*, 2006, 2008; *Cabrol et al.*, 2008]. Evidence for aqueous activity has not been seen, except as chemical alteration products and microtextures [*Cabrol et al.*, 2006; *Herkenhoff et al.*, 2006; *Ming et al.*, 2006; *Morris et al.*, 2006; *Wang et al.*, 2006a, 2006b].

[7] Surface particles along the Spirit traverse, then, are believed to have been emplaced through some combination of volcaniclastic and impact ejecta processes, with possible mass wasting on slopes [*Arvidson et al.*, 2006; *Grant et al.*, 2006a, 2006b]. Some minor alteration of consolidated surface materials is suggested subsequent to emplacement, likely in the form of mechanical wind abrasion [*Greeley et al.*, 2006] and chemical aqueous rock-fluid interactions in an acidic environment [*Squyres et al.*, 2006; *Ming et al.*, 2006; *Morris et al.*, 2006; *Wang et al.*, 2006a, 2006b]. Examining the morphology and texture of pebbles and cobbles at the landing site allows us to further test these conclusions and assess the relative efficacy of volcanic, impact and mass wasting surface processes at mm to cm scales in generating and transporting particles. We evaluate whether any sustained transport is indicated by particle morphology and to what extent, if any, in situ weathering processes have influenced particle morphology.

3. Data Collection

[8] The region traversed by Spirit is characterized by the presence of a significant number of pebble- to cobble-sized (2–256 mm [*Wentworth*, 1922]) particles. We utilized images from the clast survey, an imaging campaign designed to better systematize a study of particle characteristics and their variation with location. Particles imaged in the clast survey represent a subset of the geological units where traversing was possible for Spirit. Conclusions based on data from the clast survey images are thus biased by what constitutes trafficable terrain.

[9] The Pancam clast survey is a collection of single frame, generally two-filter images taken with the Pancam multispectral and stereoscopic camera system [*Bell et al.*, 2003, 2004] looking at an angle of 70° down from horizontal and generally 0° azimuth in the rover frame. The goal of the campaign has been to capture high-resolution details of the loose particles along transect, with as little look angle bias as possible. Images originally were planned to be taken after every rover drive; however, this plan has not always proved either practical or the most desirable use of limited rover resources. In practice, clast survey images were acquired after most long (>10 m) drives, or at least every 20–30 sols in which significant driving occurred. Large gaps in the clast survey data set can be explained by the necessity of making more mission crucial observations, or by lack of movement (e.g., the long hiatus between sol 791–1052, which Spirit spent within a few meters of the same position at the second winter over location).

[10] We examined images taken from sol 450 to sol 745, including the ascent of Husband Hill, descent to the El Dorado dune field, and the floor of the basin to the south of Husband Hill known as the Inner Basin (Figures 1 and 2). Forty-seven clast survey observations were taken during this period and of these, 44 were imaged in stereo using the two "blue" filters (432 and 436 nm band center, L7 and R1) as image pairs. Two additional locations on sols 734 and 738 were imaged with all 13 Pancam geologic filters, which we refer to here as image cubes. We assumed all images to be representative of the float population at each location they were taken. Spirit's location for each sol associated with a clast survey image was determined by *Li et al.* [2006] using Doppler radio positioning and triangulations utilizing landmarks in orbital and ground images, then corrected using rover wheel data from drives. Survey image locations are shown in Figure 2.

[11] The selection of particles to examine was constrained primarily by the Pancam resolution. Pancam has an angular resolution of 0.28 mrad/pixel. At a range to the surface of 1.5 m, this yields a practical resolution of ~0.4 mm/pixel [*Bell et al.*, 2003, 2004], the average resolution for clast survey images. This number varies very slightly as the range to the target varies. Because these variations translate to a difference in resolution from image to image of no more than 0.02 mm/pxl, for the purposes of this study the average resolution of 0.4 mm/pxl is assumed.

[12] Resolution yields a theoretical measure of the smallest object that can be resolved in a single pixel by the camera. More pragmatically, at least 3–5 pixels must comprise an object to "resolve" it in a useful scientific sense. Using images at 0.4 mm/pxl resolution, it is reasonable to assume that features on particles on the order of 1–3 mm in size may be resolved. For the purposes of assessing shape and roundness of particles, we are then limited by the size of the smallest feature that must be resolved in order to yield accurate data, in this case, a particle corner. In practice, a particle corner must be at least 5 mm in diameter (5–10 pixels) to be resolved sufficiently for roundness to be determined. Roundness is the limiting factor, as sphericity can be determined if the smallest "lobe" or protuberance is resolvable. We performed outlines of images of roundness standards [*Powers*, 1953] to determine the minimum particle size required to resolve very angular

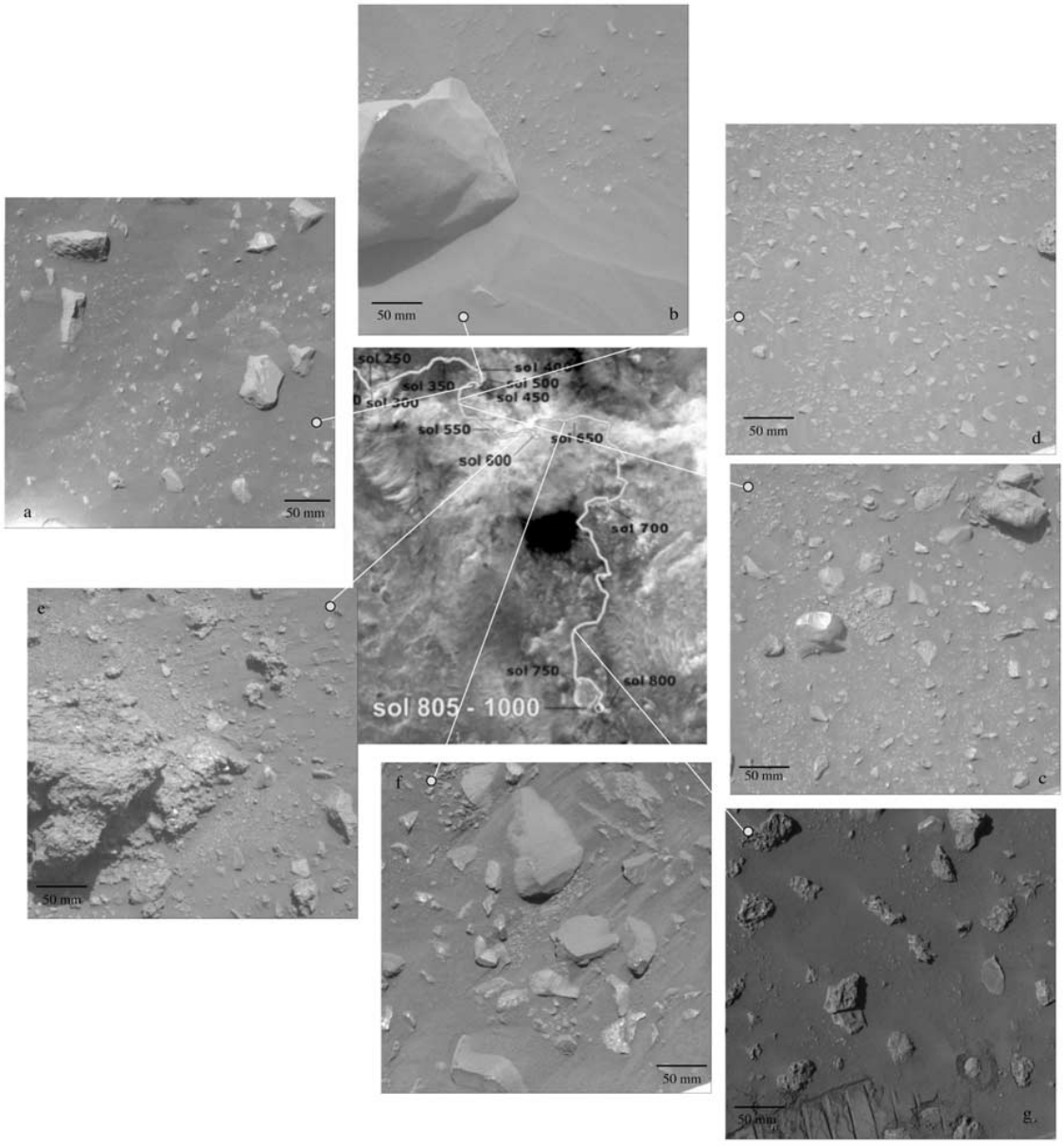

Figure 2. Spirit rover traverse overlain on orbital HiRISE image. Examples of clast survey images taken along the traverse are shown, with all clast survey sols noted. (a) Sol 456. Particle-rich image with significant amounts of mantling dust and unconsolidated material. Particles are <5–100 pixels in diameter and subangular to subrounded, with textures ranging from smooth to rough and nodular. (b) Sol 508. Moderately particle-rich image. The largest particle (Backstay) is subrounded, with flat facets ending in distinct edges. Smaller particles average 10 pixels in diameter, and appear to be rough, subangular, and relatively flat. (c) Sol 523. Particle-rich image, with knobby basement texture visible. The particle population is typical of the majority of the traverse, with flatter, smaller particles and larger, more rounded particles that have both smooth and vesicular facets. (d) Sol 525. Particle-rich image, with knobby basement texture. A single (truncated) rough-textured larger particle is visible; otherwise, the scene is dominated by bright, smooth-faceted, angular to subangular particles approximately 15–25 pixels across. (e) Sol 577. Particle-rich image with basement material. Particles are 5–100 pixels in diameter and angular to very angular, with very rough texture characterized by angular to subrounded protuberances. The large clast at lower left represents texture Type 4. (f) Sol 638. Very large, smooth-faceted, sharp-edged particles, heavily mantled in unconsolidated material that streaks from the lower left to the upper right of the images. Knobby bedrock can be seen underlying the float. (g) Sol 742. Larger vesiculated, very angular scoria and smaller smoother-faceted subangular particles interspersed with much smoother particles.

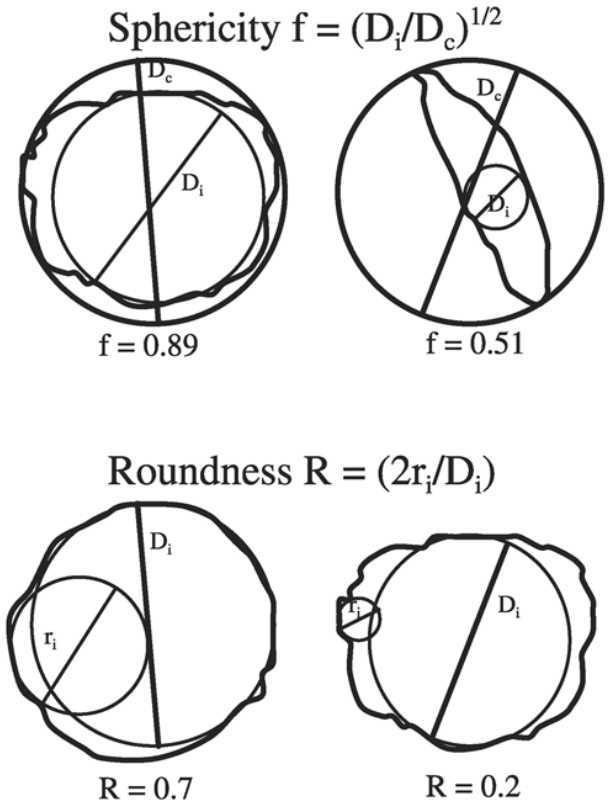

Figure 3. Schematic of the methods used for determining sphericity and roundness of particles, adapted from *Riley* [1941] and *Dobkins and Folk* [1970, derived from *Wentworth*, 1919]. The equations that utilize these variables are listed and described in the text, after *Yingst et al.* [2007].

corners, and found that particles classified as very angular must be at least 100 pixels in diameter (translating to 40–60 mm) for their sharpest corners to be resolvable (either visually or measurably) at 3–5 pixels. We thus use this as our minimum particle size for which we can determine quantitative roundness. The limit for sphericity is less stringent, as it is the overall shape of the particle that is important. We chose a conservative limit of 20–30 pixels apparent diameter (8–12 mm) as the minimum size particle for which sphericity could be measured on the basis of previous similar work with Mars Pathfinder loose particles [*Yingst et al.*, 2007].

4. Data Analysis

[13] Each clast survey image, image pair or cube was initially assessed for general characteristics, and then candidate particles were examined. All particles greater than 15 pixels (6 mm) in diameter were numbered and recorded. Those numbered particles that were truncated by the image, were partially buried by unconsolidated material, or whose outlines were otherwise obscured (e.g., by shadow or other intervening particles), were not included in subsequent analyses.

[14] Once the particle population was narrowed down to those for which useful information could be collected, roundness for each particle above the size limit was determined visually, using the standards of *Powers* [1953]. We then utilized the methodology developed and refined by *Yingst et al.* [2007] to calculate quantitative indices of macromorphology, including particle diameter (estimated as the major axis length), elongation (minor axis divided by major axis), sphericity (how closely the particle shape resembles a sphere) and roundness (sharpness of the corners of a particle).

[15] A digital tracing was made of each particle, and from this two-dimensional polygon the largest inscribed (D_i) and smallest circumscribed (D_c) circles for each particle were determined; these were used to calculate sphericity using [*Riley*, 1941]

$$f = (D_i/D_c)^{1/2}.$$

For roundness, the radius of curvature (r_i) of the smallest corner of each polygon was selected and roundness calculated by (see *Dobkins and Folk* [1970] derived from *Wentworth* [1919])

$$R_i = 2r_i/D_i.$$

This method is shown graphically in Figure 3. Minor and major axes were also calculated for each analyzed particle and divided to yield elongation values (where a larger value indicates an equant particle and a smaller value indicates a more elongate particle).

[16] Particles were also assessed and classified for texture. Surface texture describes how a particle surface varies from a perfectly flat surface at scales smaller than the corners and angles of the particle, and thus is independent from roundness. For example, both ventifacts and fluvially altered rocks at the Mars Pathfinder landing site have been classified as subangular [*Yingst et al.*, 2007]; texture is the variable that allowed these two morphologies to be separated and classified according to transport and wear. There is no commonly used method for quantifying texture on the basis of two-dimensional image data.

[17] In summary, sphericity and elongation approximate particle shape (the proportions of a particle), while roundness reflects variations at particle corners and texture reflects variations between and superimposed on corners [e.g., *Barrett*, 1980]. Together, shape, roundness and texture are metrics that are independent of each other and constitute a reasonable description of particle morphology. Morphologic parameters were compared to highlight correlations. Particles were classified using these characteristics and then placed in geologic context by comparing them to environmental factors (elevation, associated geologic units) so as to identify possible correlations.

[18] There is considerable terrestrial work demonstrating that reliable shape and roundness information can be calcu-

Table 1. Morphologic Characteristics by Texture Type[a]

	Number of Particles	Mean Size (mm)	Sphericity	Elongation	Roundness
Type 1	25	18 (10.87)	0.69 (0.07)	0.65 (0.16)	0.07 (0.02)
Type 2	629	10 (6.67)	0.73 (0.08)	0.67 (0.15)	0.15 (0.11)
Type 3	126	12.7 (8.59)	0.71 (0.09)	0.66 (0.17)	0.15 (0.15)
Type 4	40	20.5 (14.48)	0.70 (0.08)	0.69 (0.13)	0.10 (0.09)

[a]Values listed are the mean values for each characteristic. Standard deviations are shown in parentheses.

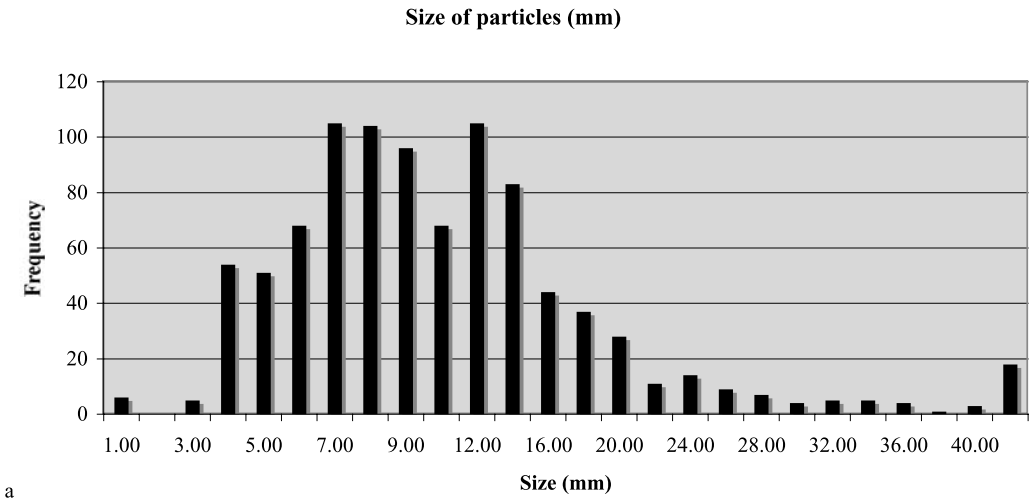

a

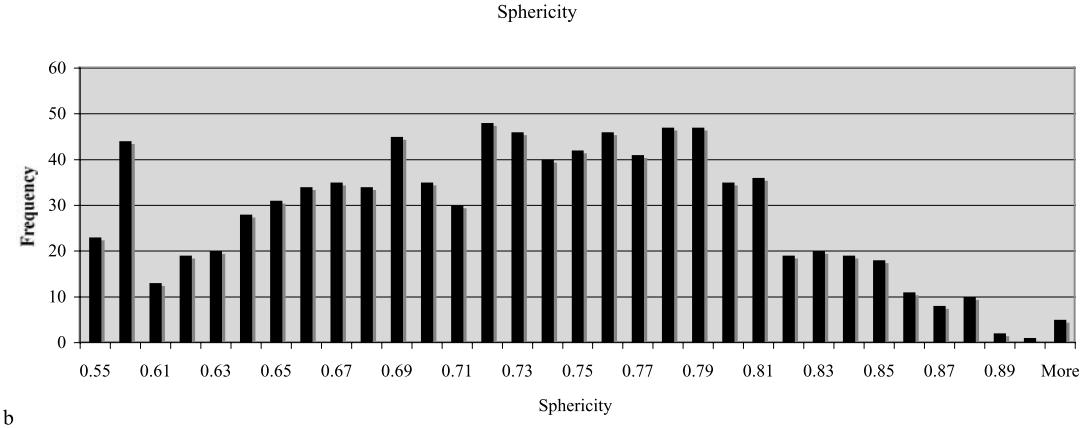

b

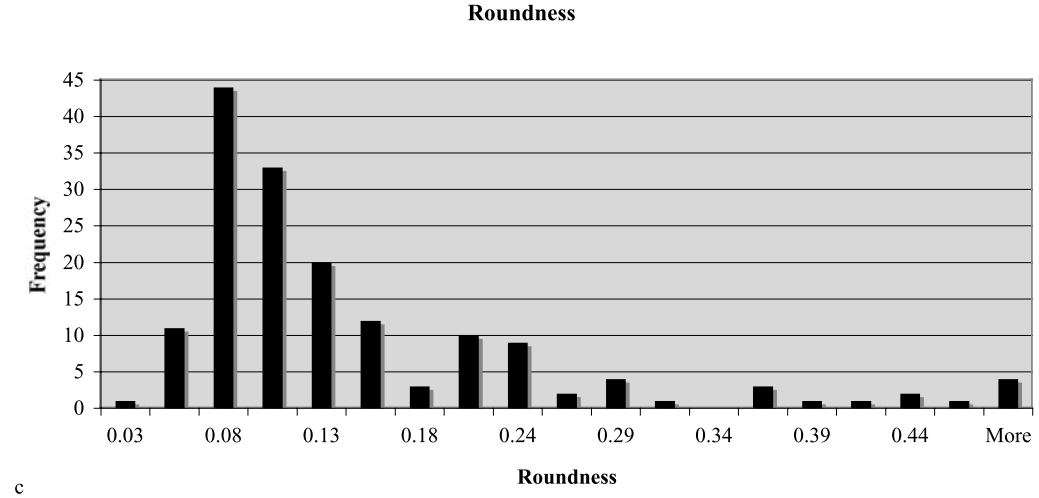

c

Figure 4. Histograms of (a) size (standard deviation 8.1); arrow indicates the size threshold for pebbles, (b) sphericity (standard deviation 0.08) and (c) roundness (standard deviation 0.12) values for all particles along the Spirit rover traverse from sol 450–750. In Figure 4a data is in mm, while Figures 4b and 4c have no units.

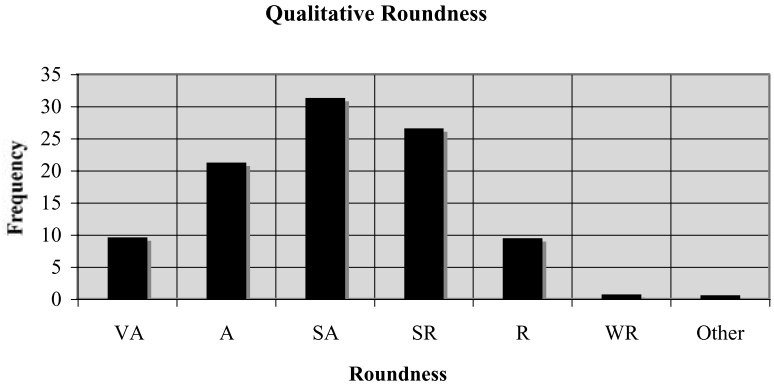

Figure 5. Histogram of qualitative roundness values for 935 particles examined in this study, shown as a percentage of total sampled particles. VA, very angular; A, angular; SA, subangular; SR, subrounded; R, rounded; WR, well rounded.

lated using only two, or in some cases, even a single dimension [e.g., *Riley*, 1941; *Cailleux*, 1947; *Kuenen*, 1956; *Sneed and Folk*, 1958; *Williams*, 1965; *Dobkins and Folk*, 1970; *Benn*, 1994]. The error introduced by approximating shape and roundness in this way has been shown to be less than 10% for pebble- to cobble-sized particles [*Riley*, 1941; *Cailleux*, 1947]. The primary source of error, then, is operator error. Accuracy in assessing shape and roundness depends on the ability of the analyst to create an accurate outline of the particle. Error introduced with respect to particle outlines was estimated by calculating the mean value of resulting morphologic indices derived by each of several operators for a test image taken on sol 545, containing 26 measurable particles. The resulting error estimate is approximately 8% for sphericity, 4% for particle size and 20% for roundness. This higher uncertainty for roundness is to be expected, as it is recognized that the curvature of a particle's sharpest corner is very difficult to determine for more angular particles [*Barrett*, 1980; *Benn*, 2004]. A population such as this, comprised primarily of subrounded to very angular particles, will introduce intrinsic uncertainties in roundness assessment.

[19] Another factor potentially influencing results is the presence of "broken" particles, that is, one segment of the particle having a significantly more curved or rounded outline than another segment. Approximately 3% of particles showed clear evidence of being fragmented in this manner. There are two possible origins for such particles: either the particles were broken in situ through a local wear process, or they were broken predeposition through a transport process [*Krumbein*, 1941a]. In some cases, the former scenario is clearly indicated (e.g., Figure 2d) because individual fragments remain. In others the origin is less clear. The presence of fragments may indicate that, as would be expected, some portion of particles have been transported through a highly energetic process [*Krumbein*, 1941a, 1941b] such as ballistic impact.

5. Results

5.1. Particle Size, Shape, and Roundness

[20] The size, sphericity, elongation and textural characteristics of 935 particles determined to be loose, unburied surface particles were examined. Additionally, 162 particles at the site were imaged at high enough resolution so that roundness could be determined. Results for all particles are summarized in Table 1, organized by texture type.

[21] Particles from below resolution to nearly 70 mm in major axis length were observed, with the smallest resolvable particle being 2.65 mm, as shown in Figure 4. All particles fell within the pebble to cobble size range [*Wentworth*, 1922], while a subset of 146 particles were 16–256 mm, a range that is often utilized in terrestrial morphology studies [e.g., *Howard*, 1992; *Miall*, 1970; *Pettijohn and Lundahl*, 1943]. Most particles were $\sim$ 7–12 mm in size. The mean particle size was 11.1 mm (median value 8.8), though the mean values for each sol ranged from 2.4 mm to 25 mm, demonstrating a partial dependency of size upon location along traverse.

[22] The mean value for particle sphericity was 0.72 (median 0.73), with a standard deviation of 0.07. Sphericity ranged from 0.49 to 0.92 but 38% of particles clustered between sphericity values of 0.72 and 0.79. The distribution of values retained a traditional bell curve, except for a peak at 0.60, where 5% of particles resided (Figure 4). For those particles in the 16–256 mm size range the mean and median sphericity were both 0.70, with a standard deviation of 0.08. For a terrestrial comparison, sphericity values of 0.70–0.77 are commonly associated with environments in which intermittent high-energy transport mechanisms are dominant (e.g., glacial activity [*Howard*, 1992], mass wasting [*Miall*, 1970], impact). For comparison, mature particles that have experienced sustained transport commonly have sphericities of 0.71–0.83 [*Krumbein and Sloss*, 1963]. The means for each sol ranged broadly from 0.54 to 0.92, again suggesting a likely dependence on location.

[23] Acquiring accurate elongation measurements depends on being able to resolve all three dimensions of a particle, more so than does sphericity. Thus, elongation values spanned a wider range than other indices. The mean elongation was 0.67 for all particles, but only 0.60 for particles 16–256 mm.

[24] The roundness mean for particles was 0.14, while the median was 0.10. Nearly 48% of all roundness values range between 0.08 and 0.11. Most particles were classified as subangular following the methodology developed by *Powers* [1953]. Qualitatively, roundness ranged from very angular to well rounded, but most particles were subangular, subrounded, or angular, as shown in Figure 5. Subangular

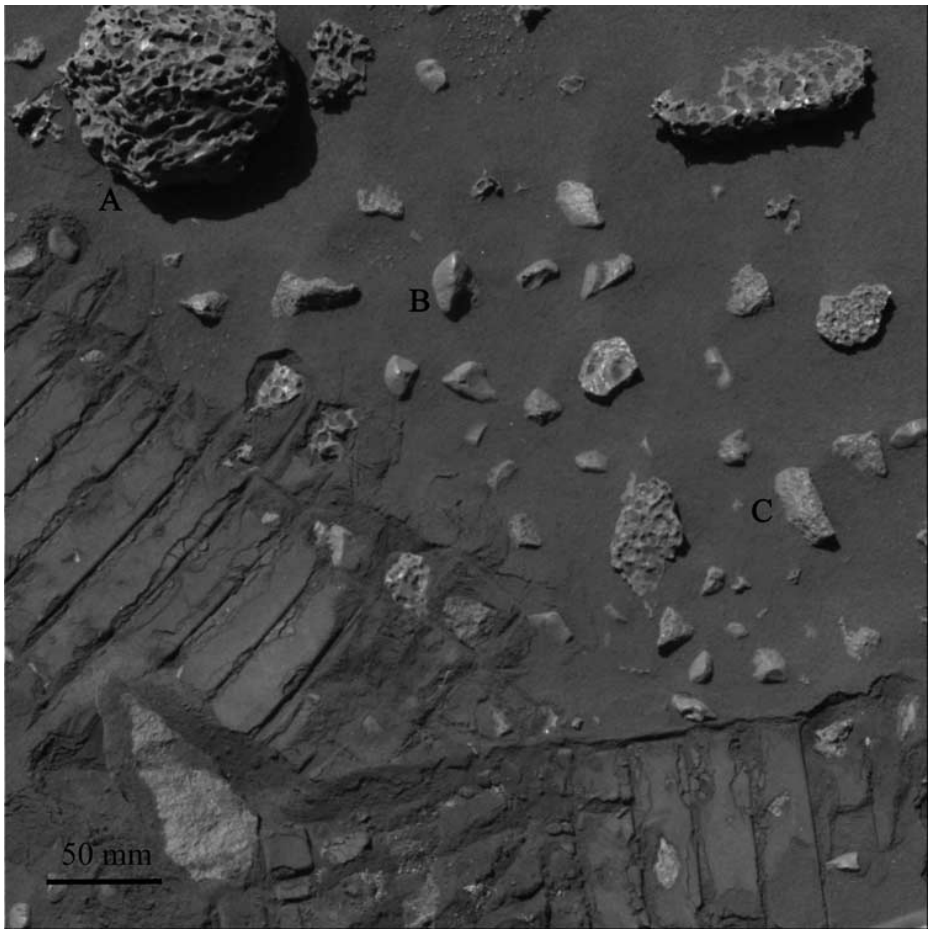

Figure 6. Pancam clast survey L7 image from sol 741. Typical of the Type 1 textural class is particle A, showing a heavily vesiculated, scoriaceous texture. Particle B is typical of the Type 2 textural class, with smooth faces and well-defined edges, with slight rounding at all corners. Particle C typifies textural class Type 3. Note that the subplanar facets similar to Type 2 are rougher and terminal edges are more irregular. Type 4 only appears in three clast survey images; this texture can be seen in Figure 2e.

particles made up 31% (289 particles) of the population, subrounded particles comprised 27% (245 particles), and 21% (196) were classified as angular. In a terrestrial setting, this combination of qualitative and quantitative results would indicate that most particles were altered by inefficient rounding mechanisms. However, a subset of scenes contained a much higher percentage of more rounded particles. These are discussed in section 7.2.

5.2. Particle Texture

[25] While atlases for texture have been developed at smaller [*Mahaney*, 2002] and larger [*Bourke and Viles*, 2007] scales and quantitative morphological textural parameters exist [*Shepard et al.*, 2001; *Wood*, 1996; *Ehlmann et al.*, 2008], these are not easily employed at the pebble to cobble size range using images alone. Thus, we adopt a straightforward Type 1–4 classification scheme for texture. Type 1 displayed a jagged, vesiculated, in many cases scoriaceous texture. A second, more common population (Type 2) was smoother than Type 1 (but not smooth), often with flat facets ending in sharp to rounded edges. Type 3 was similar to Type 2, though rougher along the flat surfaces, but commonly had more irregular edges. Finally, Type 4 was a very rough texture characterized by mm- to cm-scale angular to subrounded protuberances. Examples of each type are called out in Figure 6, as well as Figure 2e (Type 4). Locales are not uniform in terms of the number of each texture type present. Some images contained only Type 3, while others had only Type 2, and still others had varying percentages of each. Type 1 particles appeared only in postsol 733 images, while Type 4 particles appeared only between sols 551–579. Organized structure was lacking in most particles, but images taken near the Home Plate structure (sols 733 and 745), showed particles with stair-stepped edges indicative of layering.

5.3. Particle Composition

[26] Between sols 450–745, two Pancam clast surveys were taken in 13 filters, on sols 734 and 738, allowing a baseline compositional assessment to be made of particles that were also assessed for morphologic characteristics. The image from sol 738 is shown in Figure 7, along with sample spectra. The average spectral signature of particles is similar to the spectral signature of plains basalts, where variations in

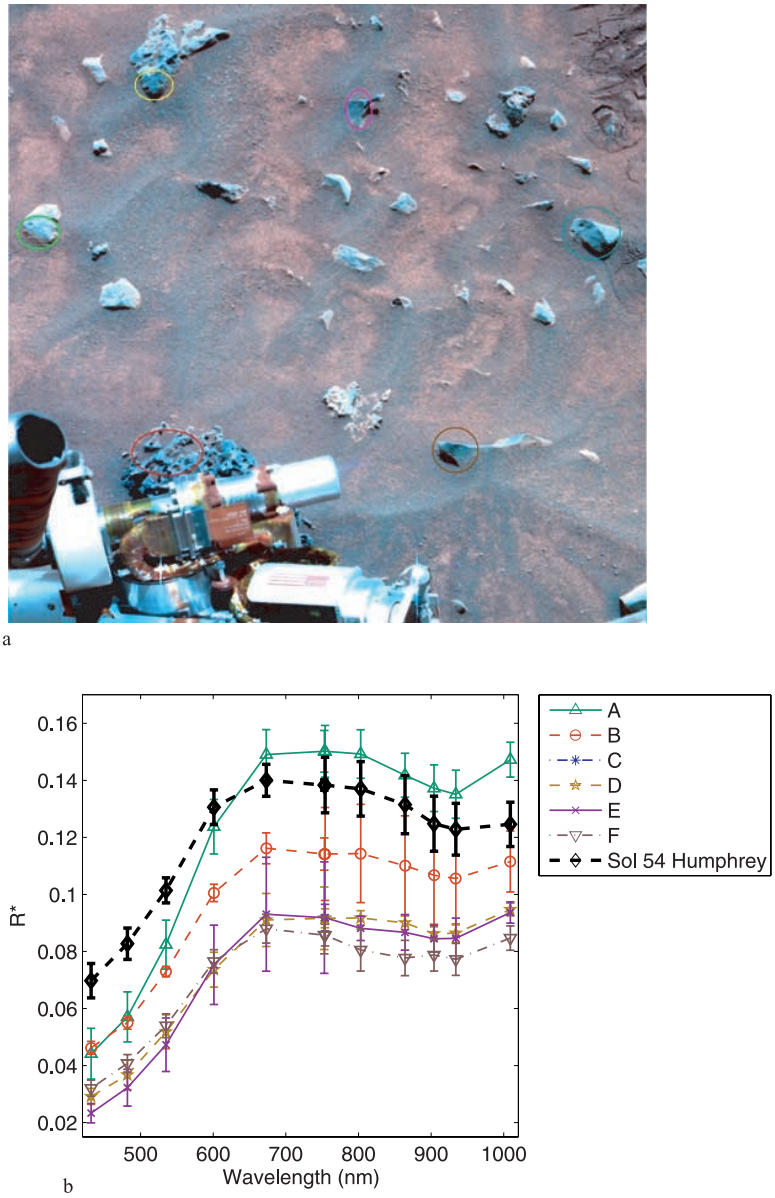

Figure 7. (a) Pancam 13-filter clast survey taken on sol 738 and (b) spectra extracted from selected particles (R^* is relative reflectance). Colored ovals in Figure 7a indicate the particle area associated with each spectrum shown; standard spectra of Humphrey, sol 54 (a plains basalts), from *Farrand et al.* [2007] are also shown for comparison.

the red/blue ratio may plausibly be equated with varying amounts of mantling dust [*Farrand et al.*, 2007]. Variations in spectral signature by texture type support this conclusion: rougher Type 1 vesicular rocks have a higher red/blue ratio (ratio of 673/482 nm bands) and higher reflectance at 535 nm than Type 2 and 3 rocks. These spectral features are both indicators of dust. Spectral signature shows no correlation with any other morphologic characteristic.

6. Analysis

6.1. Comparison of Morphologic Indices

[27] Morphologic parameters were compared to reveal any correlations between the various indices. The correlation coefficients for all variables but sphericity and elongation were close to zero. This suggests that there is no bias for any index based on particle size. The correlation coefficient between sphericity and elongation is +0.8, which is expected, as the two variables are related genetically as well as mathematically. We address sphericity alone for the remainder of this work, however, elongation values are included in this work to facilitate direct comparisons with previous work [e.g., *Garvin et al.*, 1981]. No correlation was seen between vertical elevation and any index.

6.2. Comparison and Contrast Along Traverse

[28] Landing sites on Mars have been subjected to systematic assessments of particle morphology (Viking 1 and Viking 2

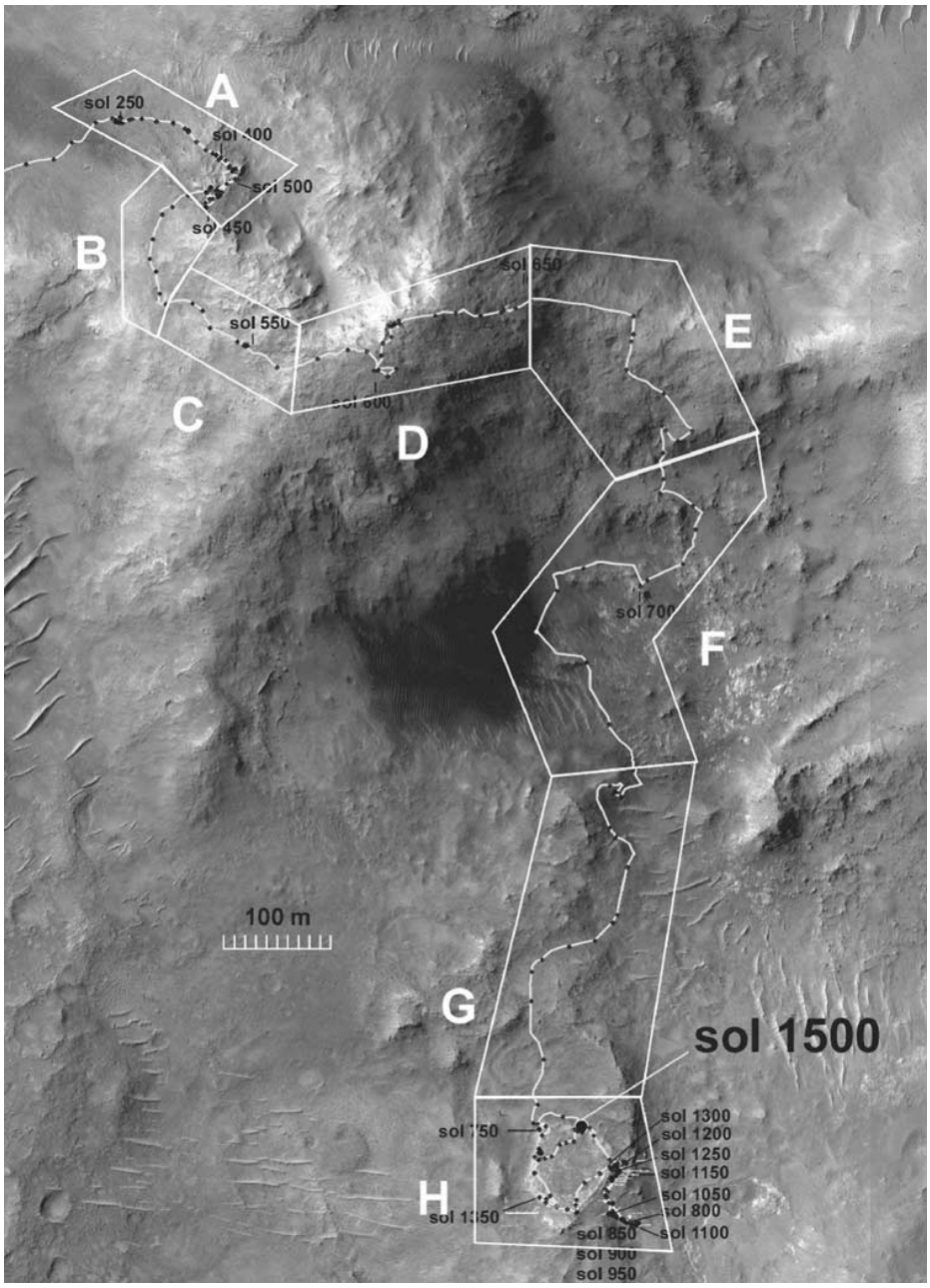

Figure 8. Spirit rover traverse across the Columbia Hills, divided into terrains distinguished by variations in slopes, outcrops, lithologies, or soil characteristics. Traverse segments are labeled A–H.

[*Garvin et al.*, 1981] and Mars Pathfinder (MPF) [*Yingst et al.*, 2007]). However, a single site can only provide a window into a single set of conditions. Where those conditions change, the site is no longer a valid representation. This is an important point, because morphology can be a powerful indicator of transport mechanisms, processes that by definition work and alter surface materials over lateral distances. Many sites throughout a region must be sampled to understand the origin and characteristics of key transport and wear processes. The MER rovers represent the first opportunity to conduct such a comprehensive assessment for a region on Mars. In the following section, we examine morphologic characteristics as mean values of each image pair or cube and assess how particle morphology and texture change along the rover traverse.

6.2.1. Morphologic Characteristics of Particles in Traverse Segments

[29] The Spirit rover traverse crosses several distinct terrains as well as lithologic classes [*Crumpler et al.*, 2006; *McCoy et al.*, 2008]. The traverse across the Columbia Hills may be segmented into several distinct terrains in which slopes, outcrops, lithologies, or soil characteristics differ from adjoining segments. Although clast survey images were not acquired at each point, there are enough to provide information regarding the nature of particle morphology for

Table 2. Morphologic Characteristics of Particles by Traverse Segment[a]

	Clast Survey Sols	Description of Terrain	Size (mm)	Sphericity	Roundness	Texture Type
Segment A (sols 250–514, 59 particles)	455, 456, 457, 506, 508	NW ascent of Husband Hill; numerous displaced Wishstone class rocks [*Squyres et al.*, 2006] and loose soils, derived from unvisited outcrops upslope; a few larger and numerous smaller particles	12.8 (8.9)	0.75 (0.07)	0.02, angular (0.11)	2, 3
Segment B (sols 515–526, 242 particles)	516, 521, 523, 525	W flank of Husband Hill; mostly displaced Wishstone class blocks of miscellaneous lithologies and abundant loose soils; particle morphology and size is highly variable	8.1 (6.0)	0.73 (0.08)	0.38, angular to subrounded (0.2)	2 (also 4)
Segment C (sols 527–577, 107 particles)	529, 545, 549, 551, 566, 574, 577	Upper W flank of Husband Hill; local outcrops of Voltaire class rocks, materials with characteristics of glassy impact breccias and melts; plentiful particles of variable roundness	15.1 (11.7)	0.70 (0.08)	0.03–0.2, very angular to subangular (0.06)	3 for sols 529–549; 4 for sols 551–577
Segment D (sols 578–654, 177 particles)	579, 582, 593, 605, 608, 615, 638, 649, 650, 652	Summit of Husband Hill; outcrops of Watchtower class lithologies along with some isolated Irvine class basalts; sol 638 has very large clasts	10.7 (6.0, few particles for sols 606 and 649)	0.74 (0.07)	0.32, subangular to subrounded (0.17)	2, 3
Segment E (sols 655–679, 106 particles)	661, 666, 679	Haskin Ridge and E flank of Husband Hill; several outcrops of massive texture and basaltic chemistry	9.8 (6.6)	0.70 (0.08)	0.1, angular to subangular (0.05)	2 (30% Type 3 for sol 666)
Segment F (sols 680–715, 59 particles)	681, 684, 689, 691, 713, 715	Haskin ridge southward past olivine-rich Comanche and El Dorado; sol 577 contains a few larger particles	10.4 (5.7)	0.69 (0.08)	0.1, angular to subangular (0.03)	4
Segment G (sols 716–742, 142 particles)	718, 720, 722, 729, 733, 734, 738, 740, 741, 742	Inner Basin, Mitcheltree Ridge and the approach to Home Plate; dominated by basalt-scoria; low variable particle roundness; variable sphericity	13.6 (8.5, no particles for sols 718, 720, and 722)	0.71 (0.1)	0.08, very angular to subangular (0.03)	1–3
Segment H (sols 743–1500, 43 particles)	743, 744, 745	Home Plate and Low Ridge and environs; all four textures are present; first appearance of Type 1	13.1 (11.2)	0.73 (0.08)	0.23, subangular to subrounded (0.09)	1

[a]Values listed are the mean values for each characteristic for the sols included in each segment. Standard deviations for each variable are shown in parentheses.

each segment. These are shown in Figure 8. Characteristics of particles in each unit are summarized in Table 2.

6.2.2. Morphologic Variability Along Traverse

[30] The mean values for size, sphericity, and roundness for each sol are shown in Figure 9. Mean particle sizes vary along traverse from 5 to 20 mm, with sols 551 and 729 having a higher maximum than this range. Most sol values are between 5 and 15 mm. Sphericity, however, varies more widely from sol to sol. Several local maxima occur that may represent geologically significant departures from other locations. These include sols 506 and 605 (sphericity is 0.79), between which exists a local minimum of 0.65 for sols 551–574 that corresponds to traverse segment D described above, as well as the only occurrence of Type 4 texture. Also noteworthy is the maximum at sol 689 (0.78), followed by a minimum of 0.67 for sol 691.

[31] Taking the mean of all roundness means per sol yields a value of 0.15 and a qualitative subangular average, but the difference from sol to sol qualitatively is greater, as the more angular classes represent a much larger range of quantitative roundness values (0.12–0.35). Additionally, some sols have a larger number of rounded particles, such as sol 521 (well embedded in traverse segment B) sol 615 and sol 744 (the sol prior to entering the Home Plate area), as shown in Figure 9c. These three clast survey image pairs represent a population of larger, Type 3 rounded particles that do not appear in other images. There are no obvious roundness minima; most values are low.

7. Discussion

7.1. Correlation of Morphology to Interpretation of Traverse Segments

[32] Because particle morphology informs our understanding of the geologic history of a region by revealing relationships between a particle's morphology and its origin and abrasion history (emplacement, transport, deposition, in situ weathering), it provides a particularly useful datapoint

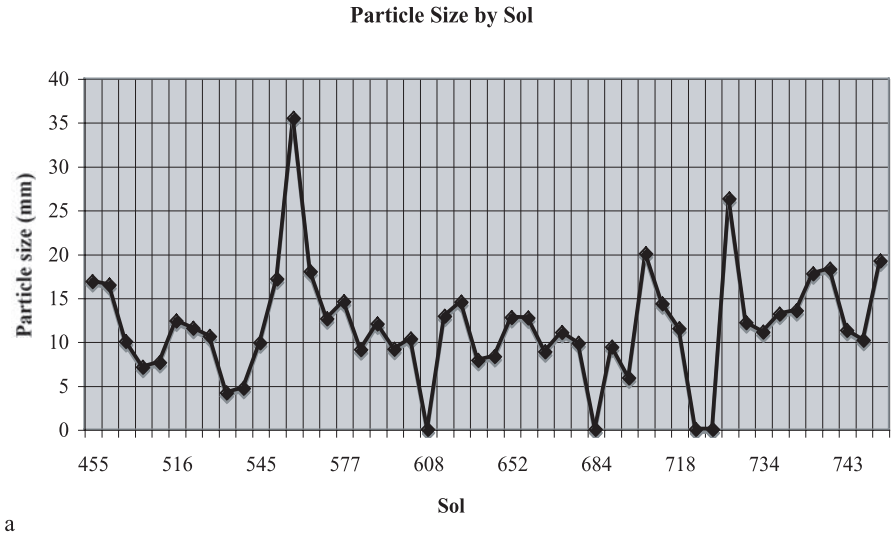

a

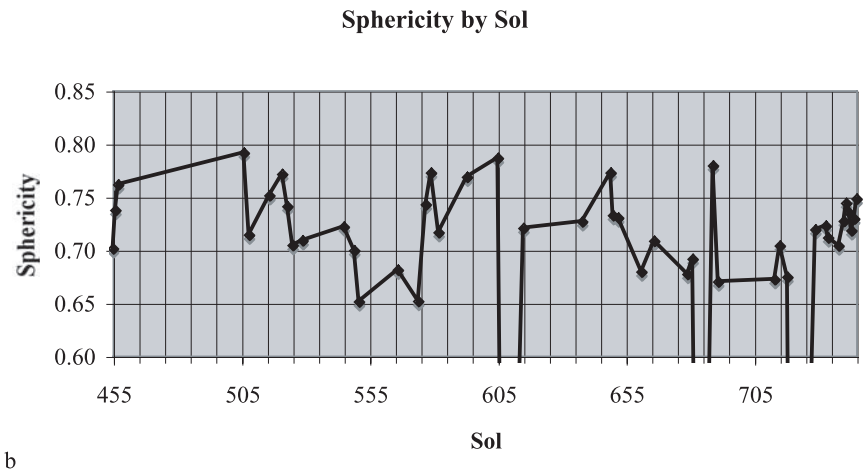

b

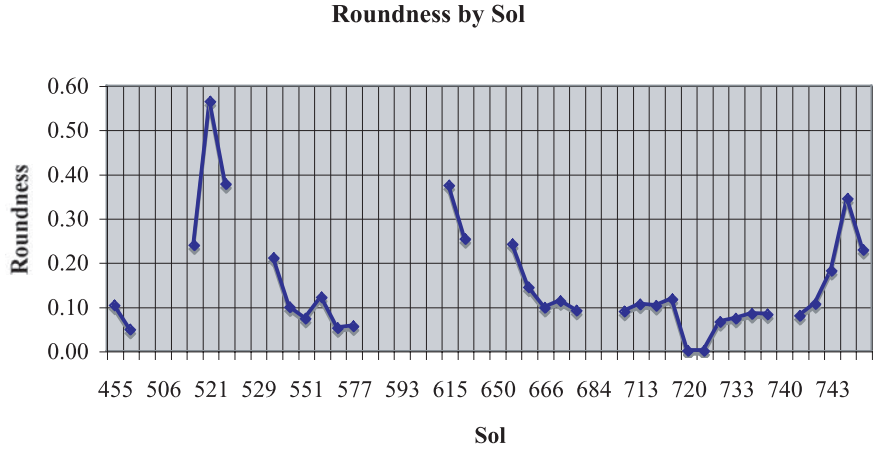

c

Figure 9. Mean values of (a) size, (b) sphericity, and (c) roundness indices graphed by sol (on the *x* axis). Note that each graph has a different scale for the *y* axis. Sols that drop off the bottom of the graph in Figure 9b and gaps in Figure 9c indicate sols for which no particles met the minimum 40 mm size threshold.

when determining the boundaries and nature of geologic units. Morphologic characteristics of surface particles that are those predicted by a proposed geologic unit provide added weight to the interpretation of units, while variant characteristics indicate that other factors may overprint geologic units or that boundaries may need to be reassessed.

Figure 10. Gray-scale image of a portion of the deposit from the 1924 Kilauea phreatic eruption, taken at similar look angle as the Pancam clast survey images. Loose particles sit atop an older, vesicular basement flow. The textures represented are similar to those seen along the Spirit rover traverse. Note the equant nature (high sphericity) of many of the particles compared to particles in Figure 2.

Microunits, regions of unusually high wear or rapid transport, such as would be associated with a mass-wasting event, may also be revealed by particle morphology.

[33] Particles vary along traverse, indicating the passage of the rover across different float regimes, consistent with crossing the preliminary geologic unit boundaries identified by *Crumpler et al.* [2006]. For example, particles imaged through traverse segment B have a high sphericity and the highest roundness (at sol 521). This argues strongly for the uniqueness of the float observed on this sol. Similarly, the transition from sol 506 (a sphericity maximum) to sol 551–574 (a minimum) corresponds to the transition between traverse segments A and C through segment B.

[34] It is not clear whether the transition in sphericity between sol 689 (0.78) and sol 691 (0.67) indicates a geologic unit transition, or perhaps denotes a microunit. However, a change of over 0.1 in sphericity for particles separated by less than 100 m in both cases suggests that these two populations may represent different transport or wear histories. Traverse segment B appears morphologically distinctive, as does segment C. The other segments are less unique morphologically, that is, the float itself is not a good indicator of the transition from one unit to another.

7.2. Identifying Primary Emplacement and Alteration Mechanisms

[35] Of the several mechanisms for particle emplacement and transport (volcanism, ballistic impact, mass wasting) or wear (eolian activity, chemical alteration) that have been suggested for Gusev, we interpret the float to be emplaced either through original volcanic activity, by subsequent disruption of volcanic deposits through ballistic impact, or a combination of both. Different float regimes are the result of multiple occurrences or mixtures of these two processes. No other transport or wear mechanism has been a significant factor in altering particle macromorphology. There are four lines of evidence that lead to this conclusion.

[36] The first line involves the values of the morphologic indices themselves. A particle begins life from outcrop with a characteristic morphology that depends on its lithology, the process by which its parent outcrop formed, and the method by which it was separated from this outcrop. From that point, however, sphericity is closely associated with the lithology (internal structure) of particles, meaning that while transport does alter the sphericity of a particle, lithology is the primary factor in determining particle sphericity. Roundness and texture are more influenced by transport and wear mechanisms that altered particles [*Folk*, 1974; *Briggs*, 1977]. Sphericity values are distributed around a single broad maximum (Figure 4). This is consistent with the hypothesis that most particles along traverse have a similar lithology, that is, the internal structure of these particles at the macroscale behaves similarly when exposed to the conditions of transport and wear represented at the site. The spectral signature of particles bears out this conclusion: all signatures compare favorably with that of plains basalts. No exotics outside this lithology are indicated, although this can only be determined for the two images from the Spirit clast survey data set.

[37] Basalt particles altered measurably by continuously acting transport (e.g., wave action, current transport, etc.) commonly display sphericities greater than 0.75 [*Krumbein and Sloss*, 1963] and roundness values greater than 0.35 that equate to subrounded or higher [*Pettijohn and Lundahl*, 1943; *Krumbein and Sloss*, 1963; *Dobkins and Folk*, 1970]. By contrast, average sphericity values that never rise above the low 0.70s and roundness values in the subangular or lower range, as seen in this study, are comparable to particles moved by intermittent high-energy transport, such as glacial till or alluvial fan deposits [*Krumbein*, 1941a; *Miall*, 1970; *Howard*, 1992], or to crushed particles [*Krumbein*, 1941b]. This result is consistent with a single lithology affected by intermittent, high-energy emplacement or modification, such as volcanism or impact.

[38] The second line of evidence is the lack of correlation between morphologic variables. The fact that there is no mathematical connection between variables indicates that no genetic connection exists among quantitative characteristics. Rather, the overall factors responsible for each morphologic index are independent of each other, implying that either several completely independent processes were active, or that particles have not been appreciably altered from their original state at formation as float. Morphology is instead related to origin and lithology rather than subsequent transport or modification.

[39] The third line of evidence is particle texture. In the comparison of particle variables shown in Table 1, particles represented by textural Types 1 and 4 tend to be larger, less spherical and less rounded. Combined with their texture, this suggests that particles in these categories began with irregular morphologies and underwent very little wear. In contrast, Types 2 and 3 are smaller, slightly more spherical and more rounded. This, along with texture, indicates that these particles either began life with less irregular morphologies, or underwent wear during or after transport. It should be noted that both Type 2 and 3 textures tend to yield angular to subangular roundness values, as the sharpness of the angles and corners are similar. This is only consistent with the former hypothesis. Particles in the clast survey images that were also imaged by the Microscopic Imager (MI) and geochemically sampled show characteristics consistent with this analysis. For example, the target Backstay (Figure 2b) displays a fine-grained texture that, along with its basaltic chemistry, implies that its origin and angularity reflect significant fragmentation and ballistic emplacement. No textural evidence of in situ weathering (e.g., flaking) was seen in any clast survey particle.

[40] The fourth line of evidence involves comparison with particle morphology at the MPF site. This comparison confirms that no secondary systematic transport or wide-scale chemical alteration significant enough to alter macromorphology is indicated. Overall mean sphericity for particles >16 mm diameter at MPF is comparable to that for similar-sized particles along the Spirit traverse [*Yingst et al.*, 2007], as would be expected for two sites dominated by basaltic float (0.72 versus 0.75). Roundness values are 0.15 compared to 0.087 for MPF. However, because corners are measured individually using the quantitative method, rather than as an overall qualitative assessment of all corners determined visually, slight variations in corner angle more easily translate into roundness variations that are highly susceptible to the size of the particle. MPF rocks are larger on average than those being sampled here by a factor of 10; for Gusev, 2% of particles are >40 mm in diameter, while at MPF 80% are >40 mm. Thus, qualitative comparisons in this case are more appropriate. The number of particles assessed as subangular or subrounded is very similar between the two sites, but angular or very angular particles appear much more frequently along the Spirit traverse. At MPF, 48% of all particles are subangular or lower, compared to 62% of particles at Gusev. This percentage is more comparable to the Viking 1 and Viking 2 sites, with 64 and 76% subangular or lower particles, respectively [*Garvin et al.*, 1981]. Thus, at MPF, where intermittent, high-energy fluvial processes have been an important factor, particle morphology shows stronger evidence of abrasion and wear than along the Spirit traverse. The implication is that MPF particles have undergone transport and wear processes that particles in this study area have not.

[41] The conclusion that particles retain to a great extent the morphology and texture of emplacement or formation is not at variance with observations of a low level of abrasion and wear within the Gusev crater region. For example, there are clear indications of eolian activity at Gusev significant enough to alter the appearance of float. *Greeley et al.* [2006] noted the presence of two types of ventifacts in Gusev, namely faceted rocks and grooves on rocks. Facets up to 1.2 m on larger rocks could be identified, with some rocks having multiple facets indicative of movement of the rock itself or multiple wind directions. Grooves were measured to be wide scallops up to 20 cm on many rocks suggesting the direction of the formative winds [*Bridges et al.*, 1999]. However, the effects of wind have not risen to the level of altering the macromorphology of pebble- to cobble-sized particles. These ventifacts are commonly cobble to boulder sized, e.g., outside the size range studied here. Neither has chemical alteration, though certainly active, been significant enough to affect quantitative results, as its appearance is not suggested at the macroscale. Thus, impact, volcanism and mass wasting remain as possible high-energy, intermittent emplacement or transport mechanisms that may have influenced particle morphology. Mass wasting can be evaluated by comparing particle populations to elevation changes. If mass wasting was a primary particle alteration process we would expect to see a higher concentration of poorly sorted particles at local elevation lows. No appreciable increase or decrease in particle frequency is noted on the basis of elevation, nor does sorting of particle texture classes appear to exist on the basis of elevation. Thus, mass wasting has not played a crucial role in particle morphology or texture in those limited areas sampled by the clast survey.

[42] By contrast, the roles of volcanism and impact have been well demonstrated. Scoriaceous particles are common at lower elevations, around the region traversed on sol 733 and later. Particles of Types 2 and 3 could plausibly be equated with volcanic deposits as well, sampling less vesicular flow interiors. If this is the case, then the first three textural populations may represent different cooling histories: particles derived from vesicular lava (Type 1 texture) and particles derived from more massive, intrusive flows (Types 2 and 3). Type 4's unusual texture likely has a more complex story. There are no appropriate terrestrial examples where a site primarily dominated by impact-related float has been characterized, though a high angularity of particles would be consistent with such a scenario. *Grant et al.* [2006a] used size-frequency distribution to demonstrate that there is little evidence for any mechanism other than impact alteration of rubbly/fractured volcanics at this site, and confirm the lack of evidence for secondary processes that altered particle size-frequency distribution.

8. Potential Role of Volcanism: Comparison With a Terrestrial Standard

[43] Particle morphology along the Spirit rover traverse can plausibly be explained as the result of ballistic transport of volcanic basalts. Our particle population is an order of magnitude smaller than that covered by *Grant et al.*

[2006a], however, and the results of the former study may not apply. We must determine if there exist any particles that retain their morphology from volcanic emplacement that could be separated from other populations, or conversely, if all float can be attributed to impact activity.

[44] Morphology derived from volcanic emplacement shares many characteristics with impact-derived float. Both particle populations result from high-energy, intermittent activity, so both share a high level of angularity and low to intermediate sphericity values (textures, by contrast, depend upon the texture of the disrupted country rock in the case of impact). Also, blocks would be expected to drape earlier units as a surface expression only. Appropriate morphological analyses have not been conducted on the morphology and texture of particle populations primarily altered either from impact or all types of volcanic deposits, so no general standard exists with which we can compare the present data. However, we conducted a first-order examination of the loose particles deposited as the result of a terrestrial phreatic eruption (the 1924 eruption of Kilauea), to determine if morphology influenced solely by this type of volcanic eruption could be distinguishable by any specific set of characteristics.

[45] We chose a phreatic eruption for comparison for several reasons. The hypothesis that groundwater might have been available in Gusev during a period of volcanic activity, to be tapped for a phreatic eruption, is supported by the presence of the Home Plate structure, thought to be a hydrovolcanic construct [*Ennis et al.*, 2007; *Schmidt et al.*, 2008, *Squyres et al.*, 2007]. Also, West Spur and Larry's Lookout rocks contain goethite and have experienced substantial alteration. Certain particles display conchoidal fracturing that would be diagnostic of glassy texture, as noted in Figure 6. Though no source vent for a phreatic eruption is visible from the position of the rover, erosion or infilling by debris might have obscured such a source. Finally, a phreatic eruption involves the disruption of previously emplaced volcanics by interaction with groundwater [*Schminke*, 2004, and references therein]. The resulting deposits consist almost exclusively of country rock, rather than juvenile material, as would occur during an impact, making it an interesting comparison to previously emplaced volcanics disrupted by external impact. We do not consider volcanic activity that might also produce loose, angular particles, but is strongly influenced by gravity, such as pyroclastic flows, since the particles in this study do not display any association with elevation.

[46] The 1924 Kilauea eruption was triggered when the level of the lava lake in Halema'uma'u Crater dropped below the water table. The walls of the crater collapsed and blocked the opening down which the lava had drained, allowing steam pressure to build up and cause violent explosions [*Jaggar and Finch*, 1924; *Decker and Christiansen*, 1984]. This eruption has three additional characteristics salient to this study: (1) the disrupted country rock shares with our study region a similar distribution, basaltic composition and mix of vesicular and nonvesicular textures; (2) the deposit is relatively young, so that the resulting particles have not been significantly worn by terrestrial weathering processes; and (3) its particles are both undisturbed and easily accessible.

[47] We examined 22 rocks associated with the deposit that are in the same size range as the Spirit rocks. We first imaged a representative section of the deposit using a similar geometry and resolution as Pancam. The analyzed scene is shown in Figure 10. Rocks within the size range of particles imaged in the clast survey were then outlined, and from these profiles size, shape and roundness were calculated. Texture was determined for all samples and results were compared to those calculated for the clast survey.

[48] The result of this first-order analysis is that the phreatic eruption produced blocks of a higher sphericity than those examined along the Spirit traverse. The sphericity of these particles had a mean value of 0.79 and a median of 0.82. High sphericity in this case may be a combined result of the rolling and abrasion of the upper scoria rubble and the plasticity of many fragments. Assuming the two sites have essentially the same bulk basaltic composition (that is, the composition fractures similarly based on gross physical properties), this indicates that the mechanism that disrupted the original country rock is not the same between the sites. The implication is that along the Spirit traverse, the rocks are primarily shaped by impact. This is consistent with the other lines of evidence noted above, which indicate that float distribution may be explained completely by impact ejecta deposition.

[49] In summary, we interpret the overall morphology and texture of particles along the Spirit traverse from sols 450–750 to be most consistent with a volcanic origin, possibly without modification, but more likely shaped and altered primarily by ballistic impact. This conclusion is important because it implies that Gusev itself may be used as a standard reference site for impact-derived morphology. Ideally, morphologic characteristics could be used to separate populations of particles formed or transported primarily from volcanic activity from those that were formed volcanically but then transported or otherwise altered through impact. The ability to separate deposits in this manner is important for understanding the contribution of impact ejecta to any local rock record. Work of this nature has focused on size-frequency distribution as judged from the surface and from orbit [*Golombek et al.*, 2003; *Grant et al.*, 2006a; *Peet et al.*, 2007] rather than examining whether particle morphology may have characteristics diagnostic of formation. Particle populations from impact and volcanic deposits have not yet been fully characterized, so these may not be used at present as standards for comparison. Here, we have determined the parameters that could represent such standards in the future.

[50] **Acknowledgments.** We gratefully acknowledge the constructive reviews of J. Zimbelman and B. Ehlmann, whose comments greatly improved this manuscript. Undergraduates Cassandra Marnocha and Zachary Christman collected portions of the data. This research was supported by the Mars Exploration Rover Program through JPL contract 1278721 to R.A.Y.

References

Arvidson, R. E., et al. (2006), Overview of the Spirit Mars Exploration Rover mission to Gusev Crater: Landing site to Backstay Rock in the Columbia Hills, *J. Geophys. Res.*, *111*, E02S01, doi:10.1029/2005JE002499.

Barrett, P. J. (1980), The shape of rock particles, a critical review, *Sedimentology*, *27*, 291–303, doi:10.1111/j.1365-3091.1980.tb01179.x.

Basilevsky, A. T., W. J. Markiewicz, N. Thomas, and H. U. Keller (1999a), Morphologies of rocks within and near the Rock Garden at the Mars Pathfinder landing site, *J. Geophys. Res.*, *104*, 8617–8636, doi:10.1029/1998JE900039.

Basilevsky, A. T., W. J. Markiewicz, N. Thomas, and H. U. Keller (1999b), Morphology of APXS-analyzed rocks at the Mars Pathfinder landing site, *Sol. Syst. Res.*, *33*, 170–186.

Bell, J. F., III, et al. (2003), Mars Exploration Rover Athena Panoramic Camera (Pancam) investigation, *J. Geophys. Res.*, *108*(E12), 8063, doi:10.1029/2003JE002070.

Bell, J. F., III, et al. (2004), Pancam multispectral imaging results from the Spirit rover at Gusev Crater, *Science*, *305*, 800–806, doi:10.1126/science.1100175.

Benn, D. I. (1994), Fabric shape and the interpretation of sedimentary fabric data, *J. Sediment. Res.*, *A64*, 910–915.

Benn, D. I. (2004), Clast morphology, in *A Practical Guide to the Study of Glacial Sediments*, edited by D. J. A. Evans, and D. I. Benn, pp. 78–92, Oxford Univ. Press, London.

Boulton, G. S. (1978), Boulder shapes and grain-size distributions of debris as indicators of transport paths through a glacier and till genesis, *Sedimentology*, *25*, 773–799, doi:10.1111/j.1365-3091.1978.tb00329.x.

Bourke, M. C., and H. A. Viles (Eds.) (2007), *A Photographic Atlas of Rock Breakdown Features in Geomorphic Environments*, 81 pp., Planet. Sci. Inst., Tucson, Ariz.

Bridges, N., et al. (1999), Ventifacts at the Pathfinder landing site, *J. Geophys. Res.*, *104*, 8595–8615, doi:10.1029/98JE02550.

Briggs, D. (1977), *Sources and Methods in Geography: Sediments*, 192 pp., Butterworths, Boston, Mass.

Cabrol, N. A., E. A. Grin, and G. Dawidowicz (1996), Ma'adim Vallis revisited through new topographic data, *Icarus*, *123*, 269–283, doi:10.1006/icar.1996.0157.

Cabrol, N. A., E. A. Grin, R. Landheim, R. O. Kuzmin, and R. Greeley (1998a), Duration of the Ma'adim Vallis/Gusev crater hydrologic system, *Icarus*, *133*, 98–108, doi:10.1006/icar.1998.5914.

Cabrol, N. A., E. A. Grin, and R. Landheim (1998b), Ma'adim Vallis evolution: Geometry and models of discharge rate, *Icarus*, *132*, 362–377, doi:10.1006/icar.1998.5903.

Cabrol, N. A., et al. (2003), Exploring Gusev Crater with MER A: Review of science objectives and testable hypotheses, *J. Geophys. Res.*, *108*(E12), 8076, doi:10.1029/2002JE002026.

Cabrol, N. A., J. D. Farmer, E. A. Grin, L. Richter, L. Soderblom, R. Li, K. Herkenhoff, G. A. Landis, and R. E. Arvidson (2006), Aqueous processes at Gusev Crater inferred from physical properties of rocks and soils along the Spirit traverse, *J. Geophys. Res.*, *111*, E02S20, doi:10.1029/2005JE002490.

Cabrol, N. A., et al. (2008), Soil sedimentology at Gusev Crater from Columbia Memorial Station to Winter Haven, *J. Geophys. Res.*, *113*, E06S05, doi:10.1029/2007JE002953.

Cailleux, A. (1947), L'indices dè émoussé des grains de sable et grès, *Rev. Geomorphol. Dyn.*, *3*, 78–87.

Crisp, J. A., M. Adler, J. R. Matijevic, S. W. Squyres, R. E. Arvidson, and D. M. Kass (2003), Mars Exploration Rover mission, *J. Geophys. Res.*, *108*(E12), 8061, doi:10.1029/2002JE002038.

Crumpler, L. S., et al. (2005a), Mars Exploration Rover geologic traverse by the Spirit rover in the plains of Gusev Crater, Mars, *Geology*, *33*, 809–812, doi:10.1130/G21673.1.

Crumpler, L. S. (2005b), MER field observations and analysis of vesicles in the Gusev Plains: Significance as records of emplacement environment, *Lunar Planet. Sci. Conf.*, *XXXVIII*, Abstract 2122.

Crumpler, L. S., and T. McCoy (2006), MER surface geologic transect mapping in the plains and in the Columbia Hills, Gusev Crater, *Lunar Planet. Sci. Conf.*, *XXXVII*, Abstract 1685.

Decker, R. W., and R. L. Christiansen (1984), *Explosive Eruptions of Kilauea Volcano, Hawaii: Explosive Volcanism: Inception, Evolution, and Hazards*, pp. 122–132, Natl. Acad. Press, Washington, D. C.

Dobkins, J. E., Jr., and R. L. Folk (1970), Shape development on Tahiti-nui, *J. Sediment. Petrol.*, *40*, 1167–1203.

Ehlmann, B. L., H. A. Viles, and M. C. Bourke (2008), Quantitative morphologic analysis of boulder shape and surface texture to infer environmental history: A case study of rock breakdown at the Ephrata Fan, Channeled Scabland, Washington, *J. Geophys. Res.*, *113*, F02012, doi:10.1029/2007JF000872.

Ennis, M. E., M. E. Schmidt, T. McCoy, W. Farrand, and N. Cabrol (2007), Hydrovolcano on Mars? A comparison of Home Plate, Gusev Crater and Zuni Salt Lake Maar, New Mexico, *Lunar Planet. Sci. Conf.*, *XXXVIII*, Abstract 1966.

Farrand, W. H., J. F. Bell III, J. R. Johnson, and D. L. Blaney (2007), Multispectral reflectance of rocks in the Columbia Hills examined by the Mars Exploration Rover Spirit: Cumberland Ridge to Home Plate, *Lunar Planet. Sci. Conf.*, *XXXVIII*, Abstract 1957.

Folk, R. L. (1974), *Petrology of Sedimentary Rocks*, Hemphill, Austin.

Garvin, J. B., P. J. Mouginis-Mark, and J. W. Head (1981), Characterization of rock populations on planetary surfaces: Techniques and a preliminary analysis of Mars and Venus, *Moon Planets*, *24*, 355–387, doi:10.1007/BF00897109.

Golombek, M. P., A. F. C. Haldemann, N. K. Forsberg-Taylor, E. N. DiMaggio, R. D. Schroeder, B. M. Jakosky, M. T. Mellon, and J. R. Matijevic (2003), Rock size-frequency distributions on Mars and implications for Mars Exploration Rover landing safety and operations, *J. Geophys. Res.*, *108*(E12), 8086, doi:10.1029/2002JE002035.

Golombek, M. P., et al. (2006), Geology of the Gusev cratered plains from the Spirit rover transverse, *J. Geophys. Res.*, *111*, E02S07, doi:10.1029/2005JE002503.

Grant, J. A., et al. (2004), Surficial deposits at Gusev Crater along Spirit rover traverses, *Science*, *305*, 807–810, doi:10.1126/science.1099849.

Grant, J. A., S. A. Wilson, S. W. Ruff, M. P. Golombek, and D. L. Koestler (2006a), Distribution of rocks on the Gusev Plains and on Husband Hill, Mars, *Geophys. Res. Lett.*, *33*, L16202, doi:10.1029/2006GL026964.

Grant, J. A., et al. (2006b), Crater gradation in Gusev Crater and Meridiani Planum, Mars, *J. Geophys. Res.*, *111*, E02S08, doi:10.1029/2005JE002465.

Greeley, R., et al. (2006), Gusev Crater: Wind-related features and processes observed by the Mars Exploration Rover, Spirit, *J. Geophys. Res.*, *111*, E02S09, doi:10.1029/2005JE002491.

Greeley, R., et al. (2008), Columbia Hills, Mars: Aeolian features seen from the ground and orbit, *J. Geophys. Res.*, *113*, E06S06, doi:10.1029/2007JE002971.

Herkenhoff, K. E., et al. (2006), Overview of the Microscopic Imager Investigation during Spirit's first 450 sols in Gusev Crater, *J. Geophys. Res.*, *111*, E02S04, doi:10.1029/2005JE002574.

Howard, J. L. (1992), An evaluation of shape indices as palaeoenvironmental indicators using quartzite and metavolcanic clasts in Upper Cretaceous to Palaeogene beach, river and submarine fan conglomerates, *Sedimentology*, *39*, 471–486, doi:10.1111/j.1365-3091.1992.tb02128.x.

Jaggar, T. A., and R. H. Finch (1924), The explosive eruption of Kilauea in Hawaii, *Am. J. Sci.*, *8*, 353–374.

Krumbein, W. C. (1941a), The effects of abrasion on the size, shape and roundness of rock fragments, *J. Geol.*, *49*, 482–520.

Krumbein, W. C. (1941b), Measurement and geological significance of shape and roundness of sedimentary particles, *J. Sediment. Petrol.*, *11*, 64–72.

Krumbein, W. C., and L. L. Sloss (1963), *Stratigraphy and Sedimentation*, pp. 106–122, W. H. Freeman, San Francisco, Calif.

Kuenen, P. H. (1956), Experimental abrasion of pebbles. Part 2. Rolling by current, *J. Geol.*, *65*, 336–368.

Kuzmin, R. O., R. Greeley, R. Landheim, N. A. Cabrol, and J. D. Farmer (2000), Geologic map of the MTM-15182 and MTM-15187 quadrangles, Gusev Crater, Ma'adim Vallis region, Mars, *U. S. Geol. Surv. Misc. Invest. Map, I-2666*.

Li, R., et al. (2006), Spirit rover localization and topographic mapping at the landing site of Gusev Crater, Mars, *J. Geophys. Res.*, *111*, E02S06, doi:10.1029/2005JE002483.

Mahaney, W. C. (2002), *Atlas of Sand Grain Surface Textures and Applications*, 237 pp., Oxford Univ. Press, Oxford, U. K.

McCoy, T., et al. (2008), Structure, stratigraphy, and origin of Husband Hill, Columbia Hills, Gusev Crater, Mars, *J. Geophys. Res.*, *113*, E06S03, doi:10.1029/2007JE003041.

Miall, A. D. (1970), Devonian alluvial fans, Prince of Wales Island, arctic Canada, *J. Sediment. Petrol.*, *40*, 556–571.

Ming, D. W., et al. (2006), Geochemical and mineralogical indicators for aqueous processes in the Columbia Hills of Gusev Crater, Mars, *J. Geophys. Res.*, *111*, E02S12, doi:10.1029/2005JE002560.

Morris, R. V., et al. (2006), Mössbauer mineralogy of rock, soil, and dust at Gusev Crater, Mars: Spirit's journey through weakly altered olivine basalt on the plains and pervasively altered basalt in the Columbia Hills, *J. Geophys. Res.*, *111*, E02S13, doi:10.1029/2005JE002584.

Peet, V. M., M. S. Ramsey, and D. A. Crown (2007), Remote sensing analyses of small terrestrial volcanic and impact craters: A Mars analog for formation, morphology and erosional processes, *Lunar Planet. Sci. Conf.*, *XXXVIII*, Abstract 2330.

Pettijohn, F. J. (1975), *Sedimentary Rocks*, pp. 282–286, Harper & Brothers, New York.

Pettijohn, F. J., and A. C. Lundahl (1943), Shape and roundness of Lake Eire beach sands, *J. Sediment. Petrol.*, *13*, 69–78.

Powers, M. (1953), A new roundness scale for sedimentary particles, *J. Sediment. Petrol.*, *25*, 117–119.

Rice, J. W., Jr., P. R. Christensen, S. W. Ruff, and J. C. Harris (2003), Martian fluvial landforms: A THEMIS perspective after one year at Mars, *Lunar Planet. Sci. Conf.*, *XXXIV*, Abstract 2091.

Riley, N. A. (1941), Projection sphericity, *J. Sediment. Petrol.*, *11*, 94–97.

Schmidt, M. E., et al. (2008), The hydrothermal origin of excess halogens at Home Plate, *J. Geophys. Res.*, *113*, E06S12, doi:10.1029/2007JE003027.

Schminke, H.-Ü. (2004), *Volcanism*, 396 pp., Springer, New York.
Shepard, M. K., B. A. Campbell, M. H. Bulmer, T. G. Farr, L. R. Gaddis, and J. J. Plaut (2001), The roughness of natural terrain: A planetary and remote sensing perspective, *J. Geophys. Res.*, *106*(E12), 32,777–32,796, doi:10.1029/2000JE001429.
Sneed, E. D., and R. L. Folk (1958), Pebbles in the lower Colorado River, Texas: A study in particle morphogenesis, *J. Geol.*, *66*, 114–150.
Squyres, S. W., et al. (2004), The Spirit rover's Athena science investigation at Gusev Crater, Mars, *Science*, *305*, 794–799, doi:10.1126/science.3050794.
Squyres, S. W., et al. (2006), Rocks of the Columbia Hills, *J. Geophys. Res.*, *111*, E02S11, doi:10.1029/2005JE002562.
Squyres, S. W., et al. (2007), Pyroclastic activity at Home Plate in Gusev Crater, Mars, *Science*, *316*, 738–742, doi:10.1126/science.1139045.
Wadell, H. (1932), Volume, shape and roundness of rock particles, *J. Geol.*, *40*, 443–451.
Wadell, H. (1933), Sphericity and roundness of rock particles, *J. Geol.*, *41*, 310.
Wang, A., et al. (2006a), Evidence of phyllosilicates in Wooly Patch, an altered rock encountered at West Spur, Columbia Hills, by the Spirit rover in Gusev Crater, Mars, *J. Geophys. Res.*, *111*, E02S16, doi:10.1029/2005JE002516.
Wang, A., et al. (2006b), Sulfate deposition in subsurface regolith in Gusev Crater, Mars, *J. Geophys. Res.*, *111*, E02S17, doi:10.1029/2005JE002513.
Wentworth, C. K. (1919), A laboratory and field study of cobble abrasion, *J. Geol.*, *27*, 507–521.
Wentworth, C. K. (1922), A scale of grade and class terms for clastic sediments, *J. Geol.*, *30*, 377–392.
Williams, E. M. (1965), A method of indicating particle shape with one parameter, *J. Sediment. Petrol.*, *35*, 993–996.
Wood, J. (1996), The geomorphological characterisation of digital elevation models, Ph.D. thesis, Univ. of Leicester, Leicester, U. K.
Yingst, R. A., A. F. C. Haldemann, K. L. Biedermann, and A. M. Monhead (2007), Quantitative morphology of rocks at the Mars Pathfinder landing site, *J. Geophys. Res.*, *112*, E06002, doi:10.1029/2005JE002582.

N. A. Cabrol, Space Science Division, NASA Ames Research Center, MS 245-3, Moffett Field, CA 94035-1000, USA.
L. Crumpler, New Mexico Museum of Natural History and Science, 1801 Mountain Road NW, Albuquerque, NM 87104, USA.
W. H. Farrand, Space Science Institute, 4750 Walnut Street, #205, Boulder, CO 80301, USA.
R. Li, Department of Civil Engineering, Ohio State University, 470 Hitchcock Hall, 2070 Niel Avenue, Columbus, OH 43210, USA.
L. D. Neakrase, School of Earth and Space Exploration, Arizona State University, Box 871404, Tempe, AZ 85287-1404, USA.
R. A. Yingst, Department of Natural and Applied Sciences, University of Wisconsin-Green Bay, 2420 Nicolet Drive, Green Bay, WI 54311, USA. (yingsta@uwgb.edu)